ASBMB
JOURNAL OF LIPID RESEARCH

rHDL modelling and the anchoring mechanism of LCAT activation

Tommaso Laurenzi[1], Chiara Parravicini[1], Luca Palazzolo[1], Uliano Guerrini[1], Elisabetta Gianazza[1], Laura Calabresi[2], Ivano Eberini[3*]

[1]Dipartimento di Scienze Farmacologiche e Biomolecolari, Università degli Studi di Milano, Via Giuseppe Balzaretti, 9, 20133, Milan, Italy

[2]Centro Enrica Grossi Paoletti, Dipartimento di Scienze Farmacologiche e Biomolecolari, Università degli Studi di Milano, Milan, Italy

[3]Dipartimento di Scienze Farmacologiche e Biomolecolari & DSRC, Università degli Studi di Milano, Via Giuseppe Balzaretti, 9, 20133, Milan, Italy

[*] Corresponding author

e-mail: ivano.eberini@unimi.it

Downloaded from www.jlr.org at BIBLIOTECA ALBERTO MALLIANI, on December 3, 2020

Running title: The anchoring mechanism of LCAT activation

ASBMB
JOURNAL OF LIPID RESEARCH

Abstract

Lecithin:cholesterol-acyl-transferase (LCAT) plays a major role in cholesterol metabolism as it is the only extracellular enzyme able to esterify cholesterol. LCAT activity is required for lipoprotein remodelling and, most specifically, for the growth and maturation of HDLs. In fact, genetic alterations affecting LCAT functionality may cause a severe reduction in plasma levels of HDL-cholesterol with important clinical consequences. Although several hypotheses were formulated, the exact molecular recognition mechanism between LCAT and HDLs is still unknown. We employed a combination of structural bioinformatics procedures to deepen the insights into the HDL-LCAT interplay that promotes LCAT activation and cholesterol esterification. We have generated a *data*-driven model of reconstituted HDL (rHDL) and studied the dynamics of an assembled rHDL::LCAT supramolecular complex, pinpointing the conformational changes originating from the interaction between LCAT and apolipoprotein A-I (apoA-I) that are necessary for LCAT activation. Specifically, we propose a mechanism in which the *anchoring* of LCAT *lid* to apoA-I helices allows the formation of a hydrophobic *hood* that expands LCAT active site and shields it from the solvent, allowing the enzyme to process large hydrophobic substrates.

Keywords: LCAT, HDL/Structure, Physical biochemistry, Cholesterol metabolism, Diseases/Dyslipidemias, Structural bioinformatics, LCAT deficiency, Molecular modelling

Downloaded from www.jlr.org at BIBLIOTECA ALBERTO MALLIANI, on December 3, 2020

ASBMB
JOURNAL OF LIPID RESEARCH

Introduction

Lecithin:cholesterol-acyl-transferase (LCAT) is a 65 kDa plasmatic protein of the α/β-hydrolase family synthesized mainly in the liver and in lower amounts also in brain, testes and kidneys. It circulates in plasma reversibly bound to lipoproteins, where it catalyzes the esterification of free cholesterol (FC) through a two-step reaction mechanism that involves the hydrolysis of a phospholipid *sn*-1 or *sn*-2 alkyl chain and its transfer to FC. Cholesteryl esters (CEs) are then removed from the surface and accumulate within the lipoproteins core, allowing the particle to store larger amounts of cholesterol. Being the only extracellular enzyme able to catalyze cholesterol esterification, LCAT plays a crucial role in the maturation, remodeling and function of lipoproteins (1,2). Although LCAT is also active on (V)LDLs, HDLs, the primary effectors of reverse cholesterol transport, are its preferential substrate and their principal protein constituent, apolipoprotein A-I (apoA-I), seems to be its strongest activator. Indeed, LCAT is required for the maturation and functionality of discoidal nascent pre-β-HDLs, that grow into spherical — mature — HDLs as they incorporate CEs produced by LCAT: while FC diffuses from the membranes of peripheral cells (including arterial walls macrophages) to nascent HDLs through the membrane ABCA1 transporter, LCAT preserves the concentration gradient by removing FC from the HDL surface (3).

Although the role of HDL in the prevention of coronary heart diseases is still debated, elucidating the role of LCAT in HDL-mediated reverse cholesterol transport remains a central issue that could aid in the treatment of cardiovascular diseases (3). Mutations in the LCAT gene lead to two rare recessive syndromes, fish-eye disease (FED) and familial LCAT deficiency (FLD), characterized by decreasing levels in LCAT residual activity. Clinical manifestations of the disease include, corneal opacity, anemia, hypoalphalipoproteinemia and alterations in blood lipids and CEs levels (4,5). In the case of FLD, alterations in HDLs maturation may result in the formation of abnormal multilamellar lipoproteins, LpX, which can cause nephropathy leading to life-threatening renal failure (6).

Downloaded from www.jlr.org at BIBLIOTECA ALBERTO MALLIANI, on December 3, 2020

While the three-dimensional structure of LCAT has been elucidated via X-ray crystallography (7–9), the complete lipid-bound structure of apoA-I is still unresolved, although several models backed up by experimental data have been proposed. Since the work of Koppaka *et al.* (1999) (10), the so-called *double belt* arrangement (opposed to the *picket-fence* model) has been established almost unambiguously. Further work by Segrest *et al.* (1999) (11) has then proposed the antiparallel LL (left-to-left) orientation of apoA-I chains with a 5/5 registry, based on computational calculations; their findings were then supported by the cross-linking/MS experiments of Silva *et al.* (2005) (12). Since then, other computational models have been proposed, showing significant differences albeit sharing the common configuration of double-belt in LL/5 registry. Notably, the *solar flare* model proposed by Wu *et al.* (2007) (13), which identified, via hydrogen-deuterium exchange experiments, solvent-exposed protruding bulges in apoA-I chains (corresponding to residues 159–180) that were proposed to activate LCAT; the *belt buckle* model, from Bhat *et al.* (2008) (14), where cross-linking/MS data were collected on 145 POPC rHDL particles, showing that N- and C-termini folded back onto apoA-I helices; the *looped belt* model, by Martin *et al.* (2006) (15), generated by performing EPR and FRET experiments on 100 POPC rHDLs, suggesting the presence of a central loop region comprised by residues 133–146. Another model was proposed by Wu *et al.* (2009) (16) in accordance with FRET, ESR and cross-linking/MS data obtained by others; this model displayed apoA-I helices spiraling around a 100 POPC cylindrical core as a *double superhelix*; however, the reliability of this model was challenged by Jones *et al.* (2010) (17) who tested the thermodynamic and kinetic stability of the double superhelix via extensive coarse-grained and simulated-annealing molecular dynamics (MD) simulations.

In the present paper, we employed a combination of computational approaches to model a reconstituted-HDL (rHDL) and analyze the structure-function relationships underlying LCAT reaction mechanism and activation mediated by apoA-I.

ASBMB JOURNAL OF LIPID RESEARCH

Downloaded from www.jlr.org at BIBLIOTECA ALBERTO MALLIANI, on December 3, 2020

ASBMB
JOURNAL OF LIPID RESEARCH

Materials and Methods

Computational procedures

Structure preparation.

LCAT structures 5BV7 and 5TXF were prepared using the "Structure preparation and refinement" panel of the Maestro program (Maestro, Schrödinger, LLC, New York, NY, 2018). Missing residues 236–242 of 5BV7 and 240–141 of 5TXF (lid-loop) were modelled using an *ab initio* method available in the module Prime of the same suite; since LCAT N- and C-termini were proven to be necessary for LCAT activity (18–20), residues 1–20 and 399–416 of both structures were also modelled. Despite the high number of residues to be modeled *ab initio*, we do not expect that inaccuracies in the predicted structure of these residues could affect our MD simulations. The PDB codes of utilized apoA-I structures are 3R2P (21), 1AV1 (22) and CNS (23).

rHDL modelling.

To generate the apoA-I all-atom model we merged structural fragments of existing templates into a *chimeric* structure. Template patches were selected considering the following properties: i) residues are in alpha-helix secondary structure, ii) suitable orientation of amphipathic helices, iii) ability to confer a circular shape to the model. We used 3R2P as the main template; the first 36 residues of the missing C-terminus helices (residues 183–218) were reconstructed from the corresponding residues of 1AV1 structure, while residues 219–243 were shaped on 3R2P central helices (residues 156–182). Residues 1–37 of 3R2P folded N-terminus (residues 1–79) were remodeled using residues from: 3R2P central helices (residues 156–182), a small fragment of the *consensus* model (CNS) and residues 44–79 of 1AV1. Structure alignment algorithms were used to correctly position residue patches using 2 to 5 overlapping residues as a guide. Energy-based homology modelling (Prime, Schrödinger, LLC, New York, NY, 2018) was used as a tool to model N- and C-termini last residues onto 3R2P residues 156–182 and to *seal* the final patched model into a continuous chain. A single apoA-I chain was modelled in this way; to model the homodimeric

Downloaded from www.jlr.org at BIBLIOTECA ALBERTO MALLIANI, on December 3, 2020

supramolecular assembly, a duplicated image of the generated chain was aligned to residues 80–182 of the antiparallel chain of 3R2P. The lipid core of the rHDL was built from an equilibrated POPC bilayer extracted from a validated MD simulation. The lipids bilayer was trimmed to a circular disk of 164 POPC molecules with a diameter of 9.2 nm and symmetrically positioned at the center of the chimeric model by aligning the coordinates of reference centers of mass. Residues within 3 Å from the phospholipidic core were minimized to avoid steric clashes (Polak-Ribiere Conjugate Gradient with convergence on RMS gradient with a threshold of 0.5).

Molecular Dynamics simulations.

All MD simulations were performed with the Desmond Molecular Dynamics System (D. E. Shaw Research, New York, NY, 2018. Maestro-Desmond Interoperability Tools, Schrödinger, New York, NY, 2018) with the following base setting: timestep for close and far interactions, 300 K Nose-Hoover thermostat, Martina-Tobias-Klein barostat with isotropic coupling and a 9.0 Å cut-off for Coulombic interactions.

Folding of the apoA-I chains around the lipid core was achieved with a 100 ns restrained MD simulation to ensure the reproducibility of the simulation and consistency towards experimental structural data. Selected atom pairs were pulled together by a flat-bottomed distance restraints with a force constant of 0.15 kcal mol^{-1} $Å^{-1}$ and a distance threshold of 7.5 ± 7.5 Å. Atom pairs sets were chosen considering data from cross-linking experiments (12,16,24,25) (**Fig.** 2, 3a). POPC residues were restrained on Z axis with a force constant of 5 kcal mol^{-1} $Å^{-1}$ to prevent the formation of a lipid drop that would have hindered hydrophobic interactions with apoA-I amphipathic helices. All restraints were removed after 100 ns and the MD was extended up to 300 ns.

Simulations of LCAT, LCAT::FAb and rHDL::LCAT complexes were all carried out with default settings.

ASBMB JOURNAL OF LIPID RESEARCH

Downloaded from www.jlr.org at BIBLIOTECA ALBERTO MALLIANI, on December 3, 2020

ASBMB
JOURNAL OF LIPID RESEARCH

Metadynamics.

A well-tempered metadynamics (wtMTD) simulation was set up to explore the energy landscape of the LCAT structure as a function of lid positioning. Two collective variables (CVs) were chosen to track the lid loop movements: 1) the dihedral angle formed by the centers of mass of the following groups: β6/β7 (214–303) and β7/αE (319–344) domains; the catalytic triad (181, 345, 377); the whole structure except the lid; the *tip* of the lid domain (232–238); 2) the distance between Cα of residues Met234 and Gly119. The height of the gaussian potential was set to 0.04 kcal mol^{-1}, with a *k*T of 5 kcal mol^{-1} and a deposition rate of 0.2 ps; a σ of 2.5° and 0.25 Å was set for the two CVs respectively. A 100.0 kcal mol^{-1} positional constraint was also applied to all Cα atoms, except for the lid loop (225–250) and the β3/αA domain (32–119), to prevent the biasing potential to affect every atom included in the CVs definition, thus ensuring values of the CVs to depend on lid positioning only. The system was prepared using the LCAT open 5TXF structure.

Abduction of a phospholipid from the surface of the rHDL towards LCAT active site was carried out using standard MTD; settings: wall 20 Å, deposition rate 1 ps, σ of 0.1 Å, height of the gaussian potential 0.3 kcal mol^{-1}. Other default MD settings were kept as reported in the Molecular Dynamics paragraph.

Protein::protein docking.

The PIPER FFT-based protein::protein docking program (licensed by Schrödinger, New York, NY, 2018) was used to dock LCAT on the final rHDL model. The last frame (300 ns) of the rHDL model from the MD simulation was minimized and set as the *receptor*, while the open- and closed-lid conformations of LCAT, obtained from the largest wtMTD minima, were set as *ligands*. Constraints were added to the docking protocol on the basis of experimental cross-linking and mutagenesis data: interactions with apoA-I residues 143–187 were favored by weighting the internal scoring function; at least one pair of residues observed in experimental cross-linking (26) were forced to stay within 12 Å. Poses were then analyzed and accepted or rejected on the basis of geometric considerations: i) proximity and orientation of LCAT active site towards phospholipid head groups, ii) contacts between LCAT β3/αA domain and lipids.

Downloaded from www.jlr.org at BIBLIOTECA ALBERTO MALLIANI, on December 3, 2020

ASBMB
JOURNAL OF LIPID RESEARCH

Results and Discussion

rHDL model

Since LCAT is active mainly on the surface of HDLs, where apoA-I is the main activator, understanding the interactions between LCAT, apoA-I and a lipid interface is crucial to picture LCAT activation and reaction mechanism. We chose to model a rHDL as this type of lipoprotein is the best simplified system to maintain general HDL properties, allowing the cross-validation between our models and experimental results.

As experimentally resolved lipid-bound apoA-I structures are currently unavailable, we relied on lipid-free apoA-I crystallographic data (21,22). We aligned residue patches of three structures, 1AV1, 3R2P and CNS to reconstruct a full-atom model of a lipid-free apoA-I poised to wrap around a lipidic core (**Fig.** 1). A mixed protocol of *restrained* and *free* MD was then used to drive the folding of the modelled apoA-I chains around the lipid core (see Methods section) (**Fig.** 3).

During the course of the simulation, apoA-I chains rearranged to better adapt to the size of the lipid core by assuming a hybrid *zig-zag* conformation and exposing hydrophobic residues towards the lipid core (**Fig.** 4a) while maintaining an 80 % α-helicity content. Computed tryptophan solvent accessible surface hindrance ($f_a = 80\%$) is also consistent with results by Guerini Rocco *et al.* 2009 (27). This measure is readily comparable with experimental data that measure, via fluorescent quenching methods, the amount of tryptophan surface area that is not exposed to the solvent. Indeed, this *accordion*-like conformation would allow apoA-I helices to stretch in order to accommodate larger amounts of lipids during HDLs maturation and growth.

ApoA-I N- and C-termini wrapped around the POPC bilayer within the first 20 ns of the simulation, as shown by the initial drop in the radius of gyration, which eventually stabilizes at 4.5 nm, consistently with literature data (27,28) (**Fig.** 3b). The root-mean-square deviation (RMSD) profile of apoA-I residues indicates that the rHDL model reached a stable conformation within the first 100 ns (**Fig.** 3c); after the

Downloaded from www.jlr.org at BIBLIOTECA ALBERTO MALLIANI, on December 3, 2020

removal of distance restraints at 100 ns, more conformations become available for the system, which converges towards a new stable conformation between 200 ns and up to the end of the simulation (**Fig.** 3g); nonetheless, distances between restrained atoms are preserved ($\langle distance \rangle$ = 14.4 Å, SD = 3.2 Å) (**Fig.** 3f).

According to root-mean-square fluctuation (RMSF) measures, the most mobile apoA-I residues are within the extremities of the N- and C-termini of both chains; while the C-terminus mobility is comparable with a common *end effect*, the increased N-terminus RMSF seems a characteristic feature also described by Jones *et al.* (2011) (29). However, residues 22–43 and 225–237 folded in a globular structure stabilized by strong electrostatic interactions: hydrogen bonds Arg27-Glu235/Glu234 (existing for 95.6 % of the simulation time), Gly26-Ser231 (58.9 %), Asn43-Gly39 (53.1 %), salt bridges Glu34-Lys238/Lys239 (78.8 % and 76.8 %), Glu234-Lys23/Arg27 (78.6 % and 74.0 %). (**Fig.** 3d). The RMSF analysis also highlighted other mobile domains in apoA-I helical structure: mobile residues 102–111 (H4), 161–169 (H6/7) and 205–221 (H8–H10) formed solvent-exposed bulges with reduced interactions with the lipid core; the elevated mobility of these regions has been previously established by limited proteolysis experiments (30), which have identified cleavage sites to be in positions compatible with our findings. Moreover, as proposed by Wu *et al.* (2007) (13), the mobility of these regions may be relevant for LCAT recognition. The poorly folded secondary structure encompassing these regions is compliant with observations from Sevugan Chetty *et al.* (2012) (31), who measured a low stability for the central amphipathic helices, indicating that these residues may be in a dynamic *unfolding and refolding* state. Another notable structural feature of this model is the formation of a tunnel in apoA-I chains in correspondence with residues 121–143 (H5) (**Fig.** 4b). This particular feature has been already observed in a previous computational experiment performed by Jones *et al.* (2009) (32), where the authors suggest that this *tunnel* may be involved in the *presentation* of substrates to LCAT. A computational study from Rocco *et al.* (2010) (33) compared the alignment of adjacent residues (143–165, H6) in natural apoA-I mutants apoA-I_{Milano} and apoA-I_{Paris}, showing that the misalignment of helices 5 and 6 due to a disulfide bridge (Cys173) in apoA-I_{Milano} mutant significantly reduces LCAT activation compared to apoA-I_{Paris}, where the antiparallel 5/5 organization is preserved, but

ASBMB JOURNAL OF LIPID RESEARCH

Downloaded from www.jlr.org at BIBLIOTECA ALBERTO MALLIANI, on December 3, 2020

the suboptimal LCAT activation of this latter mutant is likely due to Cys151 disulfide bond falling within a probable LCAT recognition site.

Assessing LCAT *lid* dynamics

We then moved on the evaluation of published LCAT structures resolved by X-ray crystallography and chose to consider 5TXF and 5BV7 as the two most representative conformations: indeed, these two crystals mainly differ by the arrangement of the *lid-loop* (residues 225–248), a key domain that regulates substrates active site accessibility (9).

While LCAT 5TXF (*closed*) structure formed crystals with an homotetrameric protein organization, 5BV7 (*open*) was crystallized in complex with an agonist antibody that enhances LCAT phospholipasic activity on soluble substrates. Although this may suggest that 5BV7 depicts LCAT in its *active* conformation, the reported *open* conformation of the lid may be artificial; in fact, a visual inspection of the surrounding crystal mates reveals that the first C-terminus residues of the adjacent structure reached into LCAT active site, forcing a wide-open conformation of the lid, as also discussed by Manthei *et al.* (2017) (9).

To test the hypothesis that the lid-loop conformation in structure 5BV7 depends on the presence of the agonist antibody, we set up two 50 ns MD simulations of 5BV7 LCAT, with and without the co-crystallized antibody fragment. The MD trajectory analyses pointed out that the *Fab-bound* LCAT simulation is the most stable, as shown by the constant RMSD profile (**Fig.** 5a); however, residues with the highest ΔRMSF between the two simulations — that is, residues that account for the highest changes in the *Fab-free* LCAT simulation — are located within LCAT β3/αA domain (**Fig.** 5b). This is also the region recognized by the Fab, indicating that the antibody actually stabilizes an otherwise highly mobile domain of LCAT.

These results suggest that the *open* arrangement of the lid observed in 5BV7 is likely not caused by the binding of the antibody fragment to LCAT β3/αA domain, therefore, in our opinion, while not necessarily a crystallographic artefact, 5BV7 is not suitable, without further refinement, to model a physiologically *active* conformation of LCAT. We compared 5BV7 to another open LCAT structure (PDB ID: 6MVD) (34)

ASBMB JOURNAL OF LIPID RESEARCH

Downloaded from www.jlr.org at BIBLIOTECA ALBERTO MALLIANI, on December 3, 2020

in complex with a small molecule activator, even if the positioning of the lid loop does not differ significantly from 5BV7 structure; in addition to that, the same crystallographic issues may still persist, in fact, an inspection of the orientation of LCAT proteins within the crystal reveals that LCAT lid loop could be forced in an open position by the surrounding crystal mates. To sample other possible lid-loop conformations we then performed a wtMTD simulation — a sampling technique which allows to describe the energy of the system as a function of reference frames, named collective variables (CVs) (**Fig.** 6a), chosen to track a particular movement —.

The free energy surface (FES) generated by the wtMTD displayed three energy wells within 3.5 kcal mol^{-1} from the global minimum (**Fig.** 6b). The structures associated with the minima of such wells correspond to an *open*, *intermediate* and a *closed* LCAT structure (**Fig.** 6c). These results indicate that energy barriers exist along the path that links the open and closed conformations and suggest that external forces may be required for the open-close transition to happen (i.e. the binding to lipoproteins). Intrigued by the identification of a metastable *intermediate* lid loop configuration, we compared it to LPLA2 lid loop (residues 209-231) (PDB ID: 4X90) (35) and found a remarkable similarity between the two structures with respect to the lid loop positioning (RMSD: 16.00 Å) albeit LCAT lid loop lacks the secondary structure element a4 alpha helix described in (35) for LPLA2 and thus exhibits a wider range of motion. It is plausible that the protrusion of the lid loop in the *intermediate* configuration may help in the interaction with lipoproteins, during which LCAT has to interact both with lipids and apoA-I residues and the lid loop has to stretch further to shield the catalytic site. Notably, the lid positioning of the *closed* conformation predicted by the wtMTD almost perfectly overlaps with the lid positioning of the 5TXF crystal structure (RMSD 5.6 Å), conversely, the lid positioning of the predicted *open* conformation shows a greater difference from the one observed in the 5BV7 crystal (RMSD 9.4 Å). Therefore, our predicted *open* LCAT structure may display a more probable and energetically favorable rearrangement of the lid-loop in solution to be used as a starting point for the rHDL-LCAT interactions simulation.

ASBMB JOURNAL OF LIPID RESEARCH

Downloaded from www.jlr.org at BIBLIOTECA ALBERTO MALLIANI, on December 3, 2020

ASBMB
JOURNAL OF LIPID RESEARCH

LCAT binds rHDLs in different positions with varying specificity

To obtain a model of an LCAT::rHDL complex, we employed a protein::protein molecular docking procedure adapted to integrate data gathered from cross-linking experiments and apoA-I mutagenesis studies; the former highlight the residues that are in proximity between LCAT and apoA-I, the latter isolate residues that, when mutated, impaired only LCAT activation while leaving ABCA1-mediated cholesterol efflux unaffected (1,26,32).

We also considered the functional characterization of LCAT glycosylation (36), which showed how the removal of the N-glycan on Asn384 improved LCAT activity on apoA-I-containing proteoliposomes, suggesting that LCAT αF helix of the α/β-hydrolase domain may be directly involved in apoA-I recognition.

Both the *open* and *closed* LCAT structures determined from the wtMTD were used as *ligands* to be docked on the rHDL model after 300 ns MD followed by minimization (for details, please, see Methods section).

When an unguided docking procedure was applied, most of the generated poses showed non-specific interactions between LCAT β3/αA domain and the phospholipidic surface of the rHDL (data not shown). However, when docking restraints were applied, more specific protein::protein interactions between LCAT and apoA-I could be observed. Experimental data suggest that LCAT may interact with rHDLs in multiple ways, in fact, not all the constraints could be satisfied simultaneously, so different existing models of the LCAT::rHDL complex can be described. We then compared the docking results to apoA-I::LCAT cross-links reported in Manthei *et al.* (2020) (37), which had not been used to guide the protein::protein docking program, and selected a subset of docking poses that could satisfy multiple interaction hypotheses. Binding poses were also shortlisted on the basis of the proximity between the β3/αA region (membrane-binding domain) and catalytic triad to phospholipids and of the presence of protein-protein interactions between LCAT and apoA-I. The selected binding poses (**Fig.** 7) were then submitted to MD simulations to assess the complex stability over time.

Downloaded from www.jlr.org at BIBLIOTECA ALBERTO MALLIANI, on December 3, 2020

In simulations 2, 3, 4 and 7, the interactions between LCAT and the rHDL are not suitable to maintain the enzyme anchored to the lipoprotein and LCAT drifts away from the complex towards the end of each simulation (**Fig.** 8a). In simulation 2, the cross-linking residue pairs LCAT Lys240 and apoA-I Lys182 (H7) are in proximity and LCAT α/β-hydrolase domain is close to H6/H7; in simulations 3 and 4, the cross-linking residue pairs LCAT Lys240 and Ser108 are close to apoA-I Lys140 and Lys118 (H5/6), while LCAT α/β-hydrolase domain contacts apoA-I H5/6; in simulation 7, no protein-protein interactions form between LCAT and apoA-I and LCAT lid loop is in a closed configuration.

However, in simulations 1, 5 and 6, despite some rearrangements in its positioning, LCAT remains bound to the rHDL with the active site facing the phospholipids. These simulations are characterized by the most negative mean interaction energy values throughout the simulation (**Fig.** 8b), indicating a higher stability of the complexes. Moreover, simulation 5 has the lowest RMSD of distances between residues that can form cross-links (37) (**Fig.** 7, caption). Protein::protein interactions occurring between LCAT and apoA-I are summarized in **Table** 1. In simulation 1, interactions between LCAT α/β-hydrolase domain and apoA-I H6 are maximized compared to the other systems, while in simulation 5 LCAT binding is localized on apoA-I H5; in simulation 6, protein-protein interactions are limited to few residues in LCAT lid loop and apoA-I H7 in favor of extensive electrostatic interactions between LCAT and the phospholipids. Despite LCAT and N- and C-termini have been described to affect LCAT binding to HDLs (9,38), we could not assign to them a role in the rHDL::LCAT interaction in any of our simulations. This is probably due to the fact that in our systems initial configurations the complex is already formed and LCAT terminal regions may be required during an earlier recognition phase; or else, the simulation time scale was too short to identify LCAT termini interactions with rHDL components given the tested starting configurations.

A possible interpretation of these data is that despite the high tendency of LCAT to form non-specific interactions when close to a lipid interface, specific protein::protein interactions are necessary to stabilize the enzyme on the lipoprotein. Protein::lipid interactions via LCAT β3/αA domain may be required to drive the first recognition then, stronger, specific, protein::protein interactions between apoA-I central helices

ASBMB JOURNAL OF LIPID RESEARCH

Downloaded from www.jlr.org at BIBLIOTECA ALBERTO MALLIANI, on December 3, 2020

and LCAT α/β-hydrolase domain are required to properly position LCAT on the lipoprotein and trigger the opening of LCAT lid, with the consequent exposure of the catalytic site.

LCAT *extracts* phospholipids from the lipoprotein surface

We speculated that LCAT could extract a phospholipid, the first substrate required for the cholesterol trans-esterification mechanism, in the same way as LPLA2 does (35), directly from the surface of the rHDL.

Simulation 6 showed a remarkable LCAT behavior: it *sits* on top of the lipid core and some interactions with apoA-I H7 keep the lid-loop in an open conformation. Because of the binding site shielding operated by the lid-loop, according to this mechanism, substrates would transit directly from the lipid surface to LCAT binding site without exposing their hydrophobic fatty acid chains to the solvent. To simulate the phospholipid *abduction* into LCAT active site, we set up a 50 ns wtMTD starting from the last frame of simulation 6; a single cv was chosen, represented by the distance between Ser181 hydroxylic group and the carboxylic carbon of the *sn-2* fatty acid chain of the closest phospholipid (**Fig.** 9a). As shown by the FES (**Fig.** 9b), there are no significant energy barriers along the reaction path, indicating that this kind of POPC transition towards LCAT active site might be favorable.

To identify a putative binding mode of the POPC residue within LCAT binding site, the frame corresponding to the lowest CV value was extracted from the wtMTD simulation; and the chemical bonds necessary to obtain the tetrahedral reaction intermediate were manually modified, the acylated enzyme structure was then optimized with a MM/GBSA method (**Fig.** 9c). Notably, during structure optimization of the acyl-enzyme, Lys218 formed a salt bridge with the phospholipid phosphate group; the role of this residue in stabilizing the substrate may explain why its mutation (Lys218Asn) results in FLD syndrome (39).

ASBMB JOURNAL OF LIPID RESEARCH

Downloaded from www.jlr.org at BIBLIOTECA ALBERTO MALLIANI, on December 3, 2020

ASBMB
JOURNAL OF LIPID RESEARCH

Conclusions

We generated an all-atom model of a reconstituted HDL making use of restrained MD by integrating experimental cross-linking and crystallographic data. The resulting model satisfied other biochemical observations, such as particle size, α-helicity content and tryptophan solvent accessibility; high-mobility regions at N- and C-termini and within apoA-I central helices were also consistent with HDX and limited proteolysis experiments. To our knowledge, this is the first time that a full-atom structure of lipid-bound apoA-I was generated from crystallographic data on the delipidated protein; the integration of cross-linking experiments into a restrained MD simulation was aimed at minimizing the biases related to the chosen starting configuration for the system, by allowing apoA-I to smoothly *fold* and rearrange itself around the lipid core instead of constraining its structure into circular double-helix belt. This approach also allowed us to deal with apoA-I N-termini without the need to guess their structure or truncate the protein sequence.

We studied and compared published LCAT crystallographic structures and an energetically stable LCAT structure in an open (active) conformation was obtained refining the experimental data with wtMTD simulations. Notably, our LCAT MD simulations show that the lid loop arrangement is decoupled from the dynamics of the membrane-binding domain, suggesting that specific interactions with apoA-I are required to stabilize an *open* configuration.

The generated rHDL model was used as a receptor to study LCAT recognition and activation mechanism. We used an integrative approach to build several models of rHDL::LCAT interactions combining data from mutagenesis and cross-linking experiments through molecular docking and then tested the dynamic behavior and the stability of the generated models with MD simulations.

Our findings on the LCAT::rHDL are complementary with the model proposed by Manthei et al. (2020) (37), where the authors integrated EM and cross-link/MS analyses to conclude that LCAT preferentially binds to helices 4/6 of apoA-I on the edge of the lipoprotein. The use of MD simulations to assess the stability of several interaction models allowed us to corroborate the importance of LCAT α/β-hydrolase

Downloaded from www.jlr.org at BIBLIOTECA ALBERTO MALLIANI, on December 3, 2020

fold and apoA-I helices 4-7 for their molecular recognition mechanism. However, we also observed that other binding modes involving LCAT membrane-binding domain are stable and could be functional to the enzyme activity. Castelijn et al. (40) simulated the binding of LCAT to a lipid bilayer coupling their MD simulations with free-energy calculations methods; our results supports their hypothesis that the main driver of the rHDL::LCAT recognition mechanism is the interaction between LCAT membrane-binding domain (β3/αA) and the lipid surface. As exemplified by simulation 6 described in this paper, we showed how less specific protein-lipid interactions indeed contribute to LCAT binding on the lipoprotein, and we further described the specific protein-protein interactions that are required to drive the opening of LCAT lid. Elaborating further on this interaction model, we then simulated the first step of LCAT reaction mechanism, showing that the extraction of a phospholipid from the rHDL lipid core occurs without having to cross significant energy barriers, resulting in the subsequent acylation of the enzyme.

We hope this work can help to support and pull together the accumulated literature on the subject of LCAT and (r)HDL interactions, as well as to address the focus of future work, which should be aimed at clarifying the functional role and the transition dynamics between the multiple binding modes that LCAT exhibits with respect to apoA-I-containing lipoproteins.

Data availability

The authors confirm that the data supporting the findings of this study are contained within the article. The raw models and molecular dynamics data are available upon request from the corresponding author (Ivano Eberini, University of Milan, ivano.eberini@unimi.it).

ASBMB JOURNAL OF LIPID RESEARCH

Downloaded from www.jlr.org at BIBLIOTECA ALBERTO MALLIANI, on December 3, 2020

Acknowledgements

The authors declare no conflict of interests. Funding was provided in part by grants from MIUR Progetto Eccellenza. IE thanks departmental 'Linea 2 – Azione A 2019' and 'National FFABR 2017 (Fondo di Finanziamento per l'Attività Base di Ricerca)'.

.

ASBMB JOURNAL OF LIPID RESEARCH

Downloaded from www.jlr.org at BIBLIOTECA ALBERTO MALLIANI, on December 3, 2020

ASBMB
JOURNAL OF LIPID RESEARCH

References

1. Jonas A. Lecithin cholesterol acyltransferase. Biochim Biophys Acta - Mol Cell Biol Lipids [Internet]. 2000;1529(1–3):245–56. Available from: http://www.sciencedirect.com/science/article/B6VNN-41T1FT7-R/1/950547bd5442395f5bec77aea588c6ce%5Cnpapers2://publication/uuid/51034E11-DC3C-4412-B527-F3075889B251

2. Asztalos BF, Schaefer EJ, Horvath K V, Yamashita S, Miller M, Franceschini G, et al. Role of LCAT in HDL remodeling: investigation of LCAT deficiency states. J Lipid Res [Internet]. 2007 Mar;48(3):592–9. Available from: http://www.jlr.org/cgi/reprint/48/3/592%5Cnhttp://dx.doi.org/10.1194/jlr.M600403-JLR200%5Cnhttp://www.ncbi.nlm.nih.gov/pubmed/?term=17183024http://www.ncbi.nlm.nih.gov/pubmed/?term=17183024http://www.ncbi.nlm.nih.gov/pubmed/?term=17183024http://www.ncbi.n

3. Ossoli A, Pavanello C, Calabresi L, Paoletti CEG. High-Density Lipoprotein, Lecithin: Cholesterol Acyltransferase, and Atherosclerosis. Endocrinol Metab. 2016;31:223–9.

4. Calabresi L, Gomaraschi M, Villa B, Omoboni L, Dmitrieff C, Franceschini G. Elevated soluble cellular adhesion molecules in subjects with low HDL-cholesterol. Arterioscler Thromb Vasc Biol. 2002;22(4):656–61.

5. Saeedi R, Li M, Frohlich J. A review on lecithin:cholesterol acyltransferase deficiency. Clin Biochem [Internet]. 2015;48(7–8):472–5. Available from: http://www.sciencedirect.com/science/article/pii/S0009912014006493

6. Ossoli A, Neufeld EB, Thacker SG, Vaisman B, Pryor M, Freeman LA, et al. Lipoprotein X Causes Renal Disease in LCAT Deficiency. PLoS One [Internet]. 2016;11(2):e0150083. Available

Downloaded from www.jlr.org at BIBLIOTECA ALBERTO MALLIANI, on December 3, 2020

from: http://www.ncbi.nlm.nih.gov/pubmed/26919698

7. Piper DE, Romanow WG, Gunawardane RN, Fordstrom P, Masterman S, Pan O, et al. The high-resolution crystal structure of human LCAT. J Lipid Res [Internet]. 2015;56(9):1711–9. Available from: http://www.jlr.org/lookup/doi/10.1194/jlr.M059873

8. Gunawardane RN, Fordstrom P, Piper DE, Masterman S, Siu S, Liu D, et al. Agonistic human antibodies binding to lecithin-cholesterol acyltransferase modulate high density lipoprotein metabolism. J Biol Chem. 2016;291(6):2799–811.

9. Manthei KA, Ahn J, Glukhova A, Yuan W, Larkin C, Manett TD, et al. A retractable lid in lecithin:cholesterol acyltransferase provides a structural mechanism for activation by apolipoprotein A-I. J Biol Chem [Internet]. 2017;(Ldl):jbc.M117.802736. Available from: http://www.jbc.org/lookup/doi/10.1074/jbc.M117.802736

10. Koppaka V, Silvestro L, Engler JA, Brouillette CG, Axelsen PH. The Structure of Human Lipoprotein A-I. J Biol Chem [Internet]. 1999 May 21;274(21):14541–4. Available from: http://www.jbc.org/lookup/doi/10.1074/jbc.274.21.14541

11. Segrest JP, Jones MK, Klon AE, Sheldahl CJ, Hellinger M, De Loof H, et al. A detailed molecular belt model for apolipoprotein A-I in discoidal high density lipoprotein. J Biol Chem. 1999;274(45):31755–8.

12. Silva RAGD, Hilliard GM, Li L, Segrest JP, Davidson WS. A mass spectrometric determination of the conformation of dimeric apolipoprotein A-I in discoidal high density lipoproteins. Biochemistry. 2005;44(24):8600–7.

13. Wu Z, Wagner MA, Zheng L, Parks JS, Shy JM, Smith JD, et al. The refined structure of nascent HDL reveals a key functional domain for particle maturation and dysfunction. Nat Struct Mol Biol. 2007;14(9):861–8.

ASBMB JOURNAL OF LIPID RESEARCH

Downloaded from www.jlr.org at BIBLIOTECA ALBERTO MALLIANI, on December 3, 2020

14. Bhat S, Sorci-thomas MG, Tuladhar R, Samuel MP, Thomas J. NIH Public Access. 2008;46(26):7811–21.

15. Martin DDO, Budamagunta MS, Ryan RO, Voss JC, Oda MN. Apolipoprotein A-I assumes a "looped belt" conformation on reconstituted high density lipoprotein. J Biol Chem. 2006;281(29):20418–26.

16. Wu Z, Gogonea V, Lee X, Wagner MA, Li XM, Huang Y, et al. Double superhelix model of high density lipoprotein. J Biol Chem. 2009;284(52):36605–19.

17. Jones MK, Zhang L, Catte A, Li L, Oda MN, Ren G, et al. Assessment of the validity of the double superhelix model for reconstituted high density lipoproteins: A combined computational-experimental approach. J Biol Chem. 2010;285(52):41161–71.

18. Vickaryous NK, Teh EM, Stewart B, Dolphin PJ, Too CKL, McLeod RS. Deletion of N-terminal amino acids from human lecithin:cholesterol acyltransferase differentially affects enzyme activity toward alpha- and beta-substrate lipoproteins. Biochim Biophys Acta [Internet]. 2003;1646(1–2):164–72. Available from: http://www.ncbi.nlm.nih.gov/pubmed/12637024

19. Lee Y-P, Adimoolam S, Liu M, Subbaiah P V., Glenn K, Jonas A. Analysis of human lecithin–cholesterol acyltransferase activity by carboxyl-terminal truncation. Biochim Biophys Acta - Lipids Lipid Metab [Internet]. 1997 Feb;1344(3):250–61. Available from: https://linkinghub.elsevier.com/retrieve/pii/S000527609600149X

20. Francone OL, Evangelista L, Fielding CJ. Effects of carboxy-terminal truncation on human lecithin:cholesterol acyltransferase activity. J Lipid Res. 1996;

21. Mei X, Atkinson D. Crystal structure of C-terminal truncated apolipoprotein A-I reveals the assembly of High Density Lipoprotein (HDL) by dimerization. J Biol Chem. 2011;286(44):38570–82.

ASBMB JOURNAL OF LIPID RESEARCH

Downloaded from www.jlr.org at BIBLIOTECA ALBERTO MALLIANI, on December 3, 2020

22. Borhani DW, Rogers DP, Engler J a, Brouillette CG. Crystal structure of truncated human apolipoprotein A-I suggests a lipid-bound conformation. Proc Natl Acad Sci U S A. 1997;94(23):12291–6.

23. Melchior JT, Walker RG, Cooke AL, Morris J, Castleberry M, Thompson TB, et al. A consensus model of human apolipoprotein A-I in its monomeric and lipid-free state. Nat Struct Mol Biol [Internet]. 2017;(November). Available from: http://www.nature.com/doifinder/10.1038/nsmb.3501

24. Pourmousa M, Song HD, He Y, Heinecke JW, Segrest JP, Pastor RW. Tertiary structure of apolipoprotein A-I in nascent high-density lipoproteins. Proc Natl Acad Sci [Internet]. 2018 May 15;115(20):5163–8. Available from: http://www.pnas.org/lookup/doi/10.1073/pnas.1721181115

25. Huang R, Silva RAGD, Jerome WG, Kontush A, Chapman MJ, Curtiss LK, et al. Apolipoprotein A-I structural organization in high-density lipoproteins isolated from human plasma. Nat Struct Mol Biol [Internet]. 2011;18(4):416–22. Available from: http://www.nature.com/doifinder/10.1038/nsmb.2028

26. Cooke AL, Morris J, Melchior JT, Street SE, Jerome WG, Huang R, et al. A Thumbwheel Mechanism for APOA1 Activation of LCAT Activity in HDL. J Lipid Res [Internet]. 2018 May 17;jlr.M085332. Available from: http://www.jlr.org/content/early/2018/05/17/jlr.M085332.full.pdf

27. Rocco AG, Gianazza E, Calabresi L, Sensi C, Franceschini G, Sirtori CR, et al. Structural features and dynamics properties of human apolipoprotein A-I in a model of synthetic HDL. J Mol Graph Model. 2009;28(4):305–12.

28. Calabresi L, Meng QH, Castro GR, Marcel YL. Apolipoprotein A-I conformation in discoidal particles: Evidence for alternate structures. Biochemistry [Internet]. 1993 Jun 29;32(25):6477–84. Available from: https://pubs.acs.org/doi/abs/10.1021/bi00076a023

ASBMB JOURNAL OF LIPID RESEARCH

Downloaded from www.jlr.org at BIBLIOTECA ALBERTO MALLIANI, on December 3, 2020

29. Jones MK, Gu F, Catte A, Li L, Segrest JP. “Sticky” and “promiscuous”, the yin and yang of apolipoprotein A-I termini in discoidal high-density lipoproteins: A combined computational-experimental approach. Biochemistry. 2011;50(12):2249–63.

30. Calabresi L, Tedeschi G, Treu C, Ronchi S, Galbiati D, Airoldi S, et al. Limited proteolysis of a disulfide-linked apoA-I dimer in reconstituted HDL. J Lipid Res [Internet]. 2001 Jun;42(6):935–42. Available from: http://www.ncbi.nlm.nih.gov/pubmed/11369801

31. Sevugan Chetty P, Mayne L, Kan Z-Y, Lund-Katz S, Englander SW, Phillips MC. Apolipoprotein A-I helical structure and stability in discoidal high-density lipoprotein (HDL) particles by hydrogen exchange and mass spectrometry. Proc Natl Acad Sci U S A [Internet]. 2012 Jul 17;109(29):11687–92. Available from: http://www.pnas.org/cgi/doi/10.1073/pnas.1209305109

32. Jones MK, Catte A, Li L, Segrest JP. Dynamics of activation of lecithin:cholesterol acyltransferase by apolipoprotein A-I. Biochemistry. 2009;48(47):11196–210.

33. Rocco AG, Sensi C, Gianazza E, Calabresi L, Franceschini G, Sirtori CR, et al. Structural and dynamic features of apolipoprotein A-I cysteine mutants, Milano and Paris, in synthetic HDL. J Mol Graph Model [Internet]. 2010;29(3):406–14. Available from: http://dx.doi.org/10.1016/j.jmgm.2010.08.002

34. Manthei KA, Yang S, Baljinnyam B, Chang L, Glukhova A. Molecular basis for activation of lecithin : cholesterol acyltransferase by a compound that increases HDL cholesterol. 2018;2:1–61.

35. Glukhova A, Hinkovska-Galcheva V, Kelly R, Abe A, Shayman JA, Tesmer JJG. Structure and function of lysosomal phospholipase A2 and lecithin:cholesterol acyltransferase. Nat Commun [Internet]. 2015;6:6250. Available from: http://www.nature.com/doifinder/10.1038/ncomms7250

36. O K, Hill JS, Wang X, McLeod R, Pritchard PH. Lecithin:cholesterol acyltransferase: role of N-linked glycosylation in enzyme function. Biochem J [Internet]. 1993 Sep 15;294(3):879–84.

ASBMB JOURNAL OF LIPID RESEARCH

Downloaded from www.jlr.org at BIBLIOTECA ALBERTO MALLIANI, on December 3, 2020

Available from: https://portlandpress.com/biochemj/article/294/3/879/30044/Lecithincholesterol-acyltransferase-role-of

37. Manthei KA, Patra D, Wilson CJ, Fawaz M V., Piersimoni L, Shenkar JC, et al. Structural analysis of lecithin:cholesterol acyltransferase bound to high density lipoprotein particles. Commun Biol [Internet]. 2020;3(1). Available from: http://dx.doi.org/10.1038/s42003-019-0749-z

38. Vickaryous NK, Teh EM, Stewart B, Dolphin PJ, Too CKL, McLeod RS. Deletion of N-terminal amino acids from human lecithin:cholesterol acyltransferase differentially affects enzyme activity toward α- and β-substrate lipoproteins. Biochim Biophys Acta - Proteins Proteomics [Internet]. 2003 Mar;1646(1–2):164–72. Available from: https://linkinghub.elsevier.com/retrieve/pii/S1570963903000050

39. Calabresi L, Pisciotta L, Costantin A, Frigerio I, Eberini I, Alessandrini P, et al. The molecular basis of lecithin: Cholesterol acyltransferase deficiency syndromes: A comprehensive study of molecular and biochemical findings in 13 unrelated Italian families. Arterioscler Thromb Vasc Biol. 2005;25(9):1972–8.

40. Casteleijn MG, Parkkila P, Viitala T, Koivuniemi A. Interaction of lecithin-cholesterol acyltransferase with lipid surfaces and apolipoprotein A-I derived peptides. J Lipid Res. 2018;59.

ASBMB JOURNAL OF LIPID RESEARCH

Downloaded from www.jlr.org at BIBLIOTECA ALBERTO MALLIANI, on December 3, 2020

ASBMB
JOURNAL OF LIPID RESEARCH

Tables

rHDL	LCAT	existence %
Simulation 1		
Hydrogen bonds		
TYR 100	GLN 229	26.59
LYS 118	GLY 374	22.85
ASP 150	ASN 379	21.63
LYS 118	GLN 376	19.92
ASP 103	LYS 240	18.26
ARG 151*	GLN 376	17.01
Salt bridges		
ASP 103*	LYS 240	48.59
LYS 106	ASP 335	12.39
Simulation 5		
Hydrogen bonds		
ARG 123	ASP 335	58.92
GLN 132	ASN 228*	29.44
GLU 139	GLY 119	22.14
LYS 133	LEU 70	22.04
Salt bridges		
ARG 123	ASP 335	62.60
ARG 116	ASP 328	21.23
LYS 140	ASP 113	16.46
Simulation 6		
Hydrogen bonds		
LIP	ARG 244	50.70
LIP	TYR 111*	45.80
LIP	GLU 241	33.62
LIP	HIS 122	32.22
LIP	GLN 126	28.42
LIP	SER 114	27.07
LIP	THR 59	53.54
LIP	ASN 65	25.92
LIP	TYR 111	24.73
LIP	HIS 122	23.78
LIP	ASN 65	22.73
GLU 179	LYS 240	36.11
GLU 183	LYS 238	14.09
Salt bridges		
GLU 179	LYS 240	90.31
GLU 183	LYS 238	61.44
GLU 179	LYS 238	26.47
LIP	CYS 50	21.78

Table 1: *rHDL::LCAT interactions* — the existence of protein-protein interactions with respect to total simulation time is reported. Stars indicate residues associated to FED/FLD (LCAT) or that disrupt LCAT binding/activation when mutated (apoA-I).

Downloaded from www.jlr.org at BIBLIOTECA ALBERTO MALLIANI, on December 3, 2020

ASBMB
JOURNAL OF LIPID RESEARCH

Figures

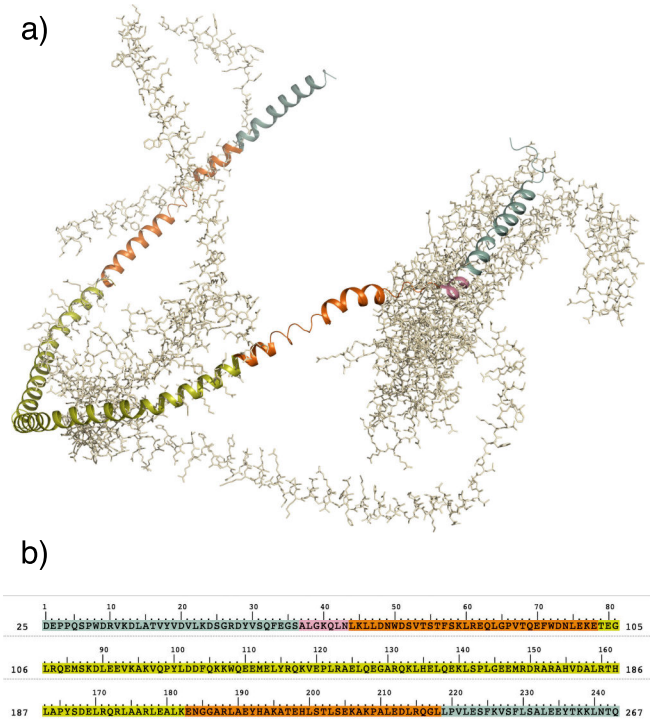

Figure 1: *ApoA-I chimeric model* — a) Ribbon representation of the patched apoA-I chimeric model; residues not used in the model generation are shown in light gray; b) color coded apoA-I primary structure. Color code: 3R2P green, homology model blue, 1AV1 orange, CNS pink.

Downloaded from www.jlr.org at BIBLIOTECA ALBERTO MALLIANI, on December 3, 2020

ASBMB
JOURNAL OF LIPID RESEARCH

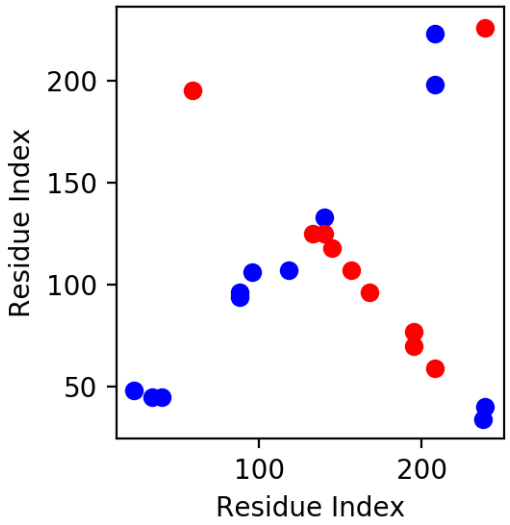

Figure 2: *apoA-I cross link map* — Inter-chain cross-links (red), intra-chain cross-links (blue).

Downloaded from www.jlr.org at BIBLIOTECA ALBERTO MALLIANI, on December 3, 2020

ASBMB
JOURNAL OF LIPID RESEARCH

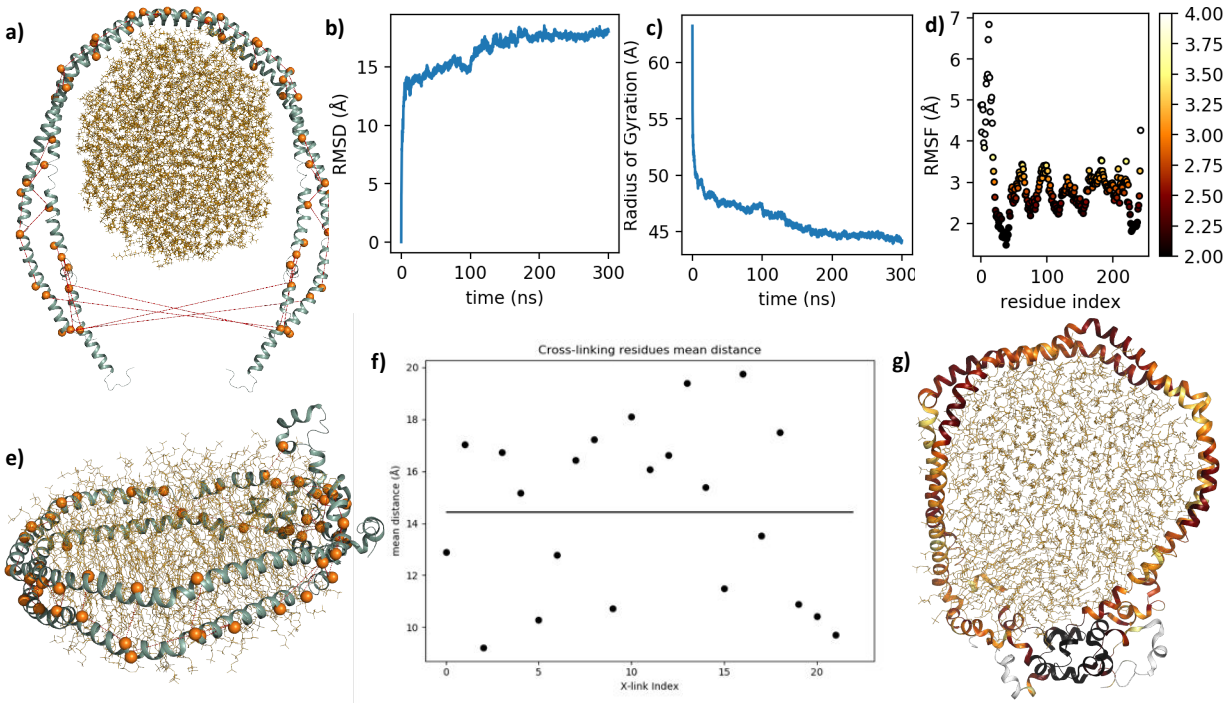

Figure 3: *apoA-I folding* — a) 3D structure of raw apoA-I model at t = 0 ns, spheres and dashed lines represent cross-linking atoms; b) RMSD plot; c) Radius of Gyration; d) RMSF plot; e) apoA-I model at t = 100 ns (before the removal of distance restraints), spheres and dashed lines represent cross-linking atoms; f) Restrained atom pairs mean distance after constraints removal. g) model at t = 300 ns, ribbon representation is color-coded on RMSF (d).

Downloaded from www.jlr.org at BIBLIOTECA ALBERTO MALLIANI, on December 3, 2020

ASBMB
JOURNAL OF LIPID RESEARCH

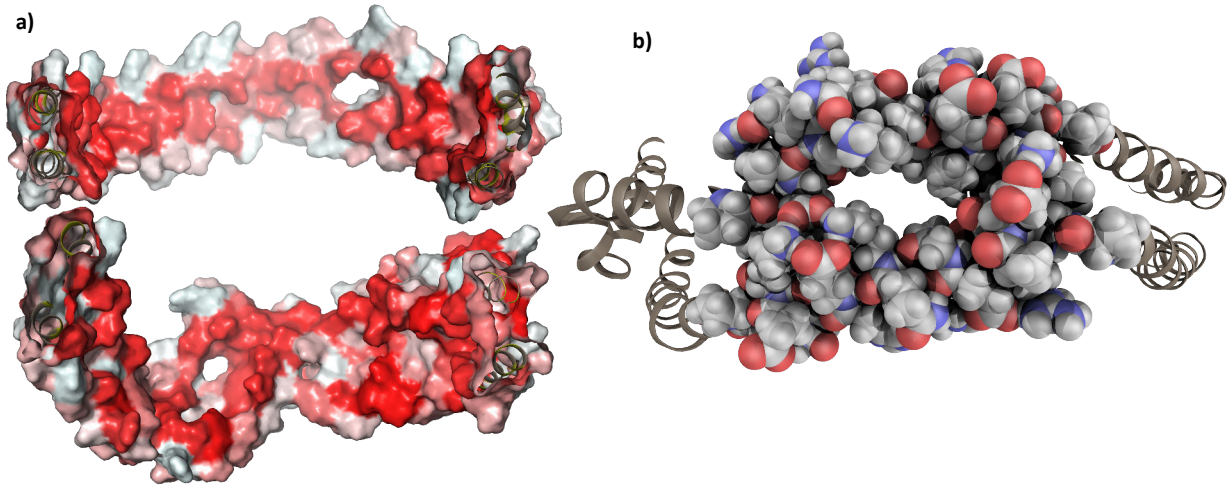

Figure 4: *apoA-I structural features* — a) Split view of apoA-I inner hydrophobic surfaces (red scale), viewed from the inside of the lipoprotein, central helices (above), termini (below); b) Van der Waal spheres view of the H5 *tunnel* located between residues 121–143 of apoA-I.

Downloaded from www.jlr.org at BIBLIOTECA ALBERTO MALLIANI, on December 3, 2020

ASBMB
JOURNAL OF LIPID RESEARCH

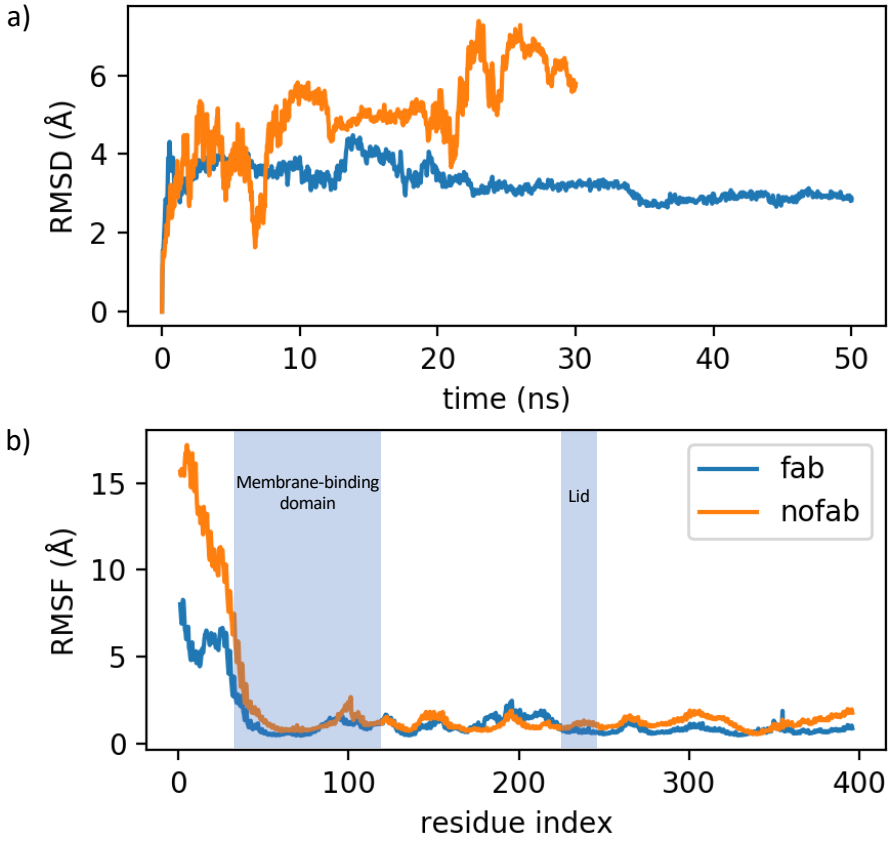

Figure 5: *LCAT MD* — comparison of residues mobility between two LCAT (5BV7) MD simulations with (blue line) and without (orange line) the co-crystallized agonistic antibody: a) RMSD plot; b) RMSF plot, lid loop is comprised between residues 225–250, within this region $RMSF_{fab} - RMSF_{nofab} = -0.075$ Å, indicating that there's no significant difference between the mobility of the lid-loop in the two simulations.

Downloaded from www.jlr.org at BIBLIOTECA ALBERTO MALLIANI, on December 3, 2020

ASBMB
JOURNAL OF LIPID RESEARCH

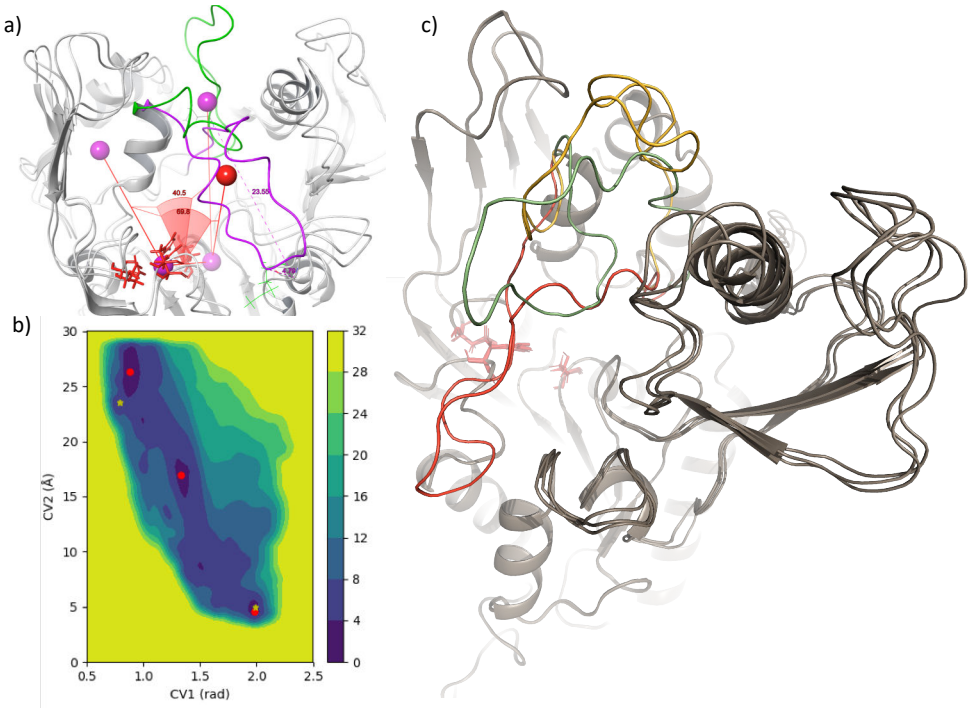

Figure 6: *LCAT wtMTD* — a) Collective variables definition: CV1 is the dihedral angle defined by the following atom groups: 1) center of mass of Cap domain 2) center of mass of catalytic triad 3) center of mass of the entire protein except the lid-loop 4) center of mass of the lid-loop; CV2 is the distance between C of Met234 and Gly119; b) Free energy surface map as a function of collective variables, red dots indicate relative minima, yellow stars indicate the value of the CVs as in 5TXF and 5BV7 crystallographic structures; c) LCAT structures corresponding to the three relative minima indicated in b), closed (red), intermediate (green), open (yellow).

Downloaded from www.jlr.org at BIBLIOTECA ALBERTO MALLIANI, on December 3, 2020

ASBMB
JOURNAL OF LIPID RESEARCH

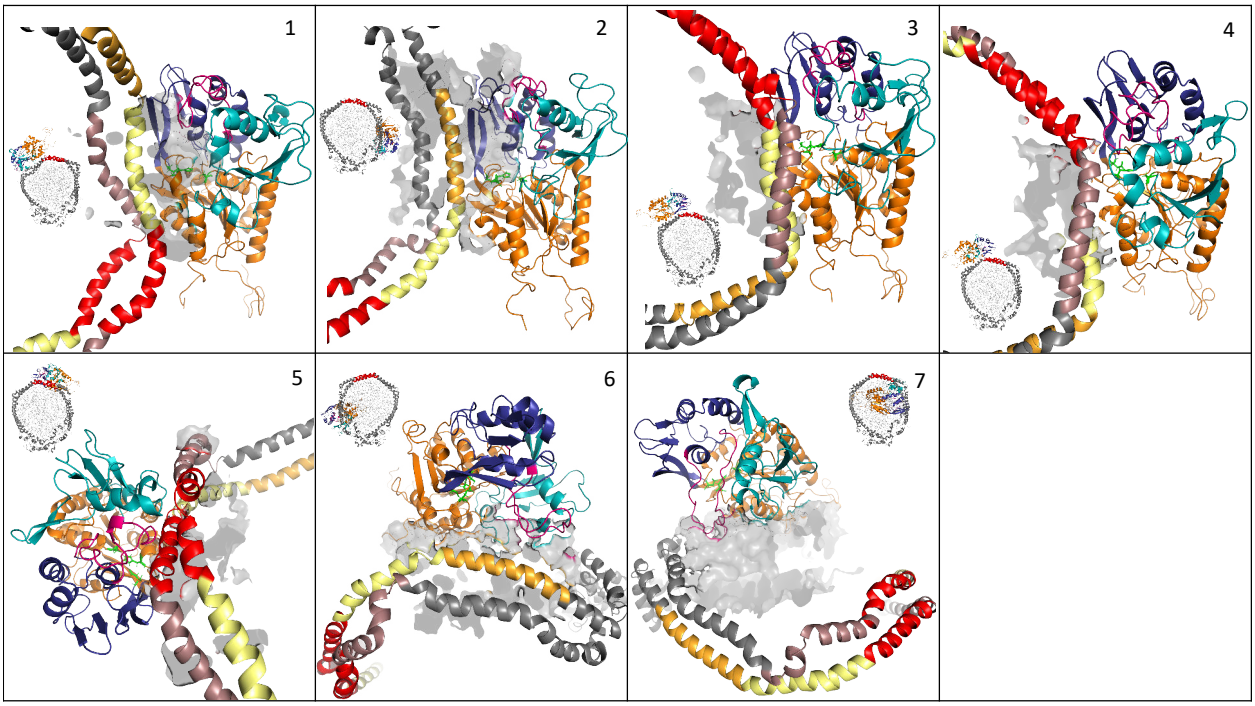

Figure 7: *rHDL::LCAT binding modes* — Results of rHDL-LCAT protein-protein docking. Binding poses differ on the basis of the number of constraints satisfied simultaneously. Color code: apoA-I (gray), H4 (pink), H5 (red), H6 (pale yellow), H7 (dark yellow), LCAT α/β-hydrolase fold (orange), lid loop (purple), membrane-binding domain (cyan), cap domain (dark blue), catalytic triad (green sticks), lipids (gray hollow surface). Each figure depicts a small overview of LCAT position with respect to the lipoprotein and a close-up view of the interaction interface. 1) maximized interactions between LCAT α/β-hydrolase domain and apoA-I H6; 2) LCAT Lys240 close to apoA-I Lys182, LCAT α/β-hydrolase domain is close to H6/H7; 3-4) LCAT Lys240 and Ser108 are close to apoA-I Lys140 and Lys118, LCAT α/β-hydrolase domain is contacts apoA-I H5/6; 5) maximized proximity between LCAT Lys240 and Ser108 and apoA-I Lys140 and Lys118 (on both chains), interaction is localized on apoA-I H5; 6) maximized interactions between LCAT and rHDL phospholipid surface, LCAT Lys240 is proximal to apoA-I Lys182 (H7); 7) closed LCAT structure, no protein-protein contacts. Cumulative RMSD between cross-linking atom pairs (Cα): **1** 54.44 Å, **2** 73.89 Å, **3** 53.17 Å, **4** 53.59 Å, **5** 47.49 Å, **6** 70.48 Å, **7** 60.58 Å.

Downloaded from www.jlr.org at BIBLIOTECA ALBERTO MALLIANI, on December 3, 2020

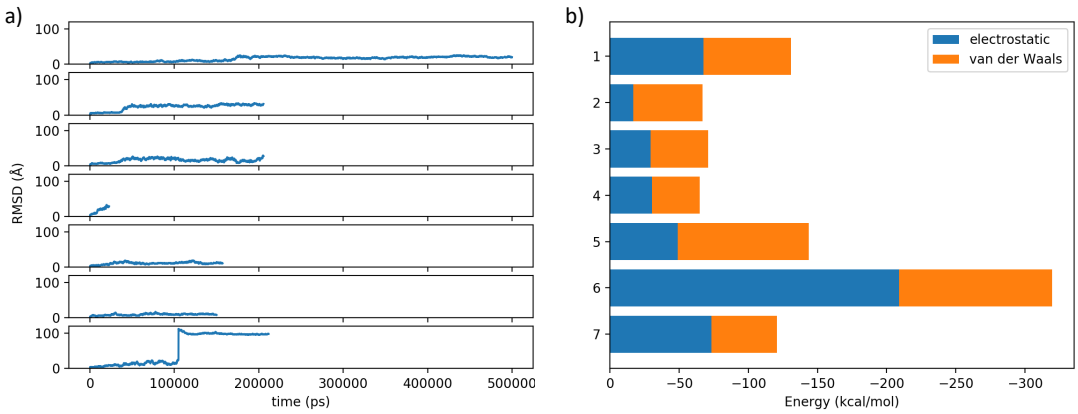

Figure 8: *rHDL::LCAT MD* — a) RMSD of LCAT fit on apoA-I; b) Mean LCAT::rHDL binding energy throughout the simulation.

Downloaded from www.jlr.org at BIBLIOTECA ALBERTO MALLIANI, on December 3, 2020

ASBMB JOURNAL OF LIPID RESEARCH

ASBMB
JOURNAL OF LIPID RESEARCH

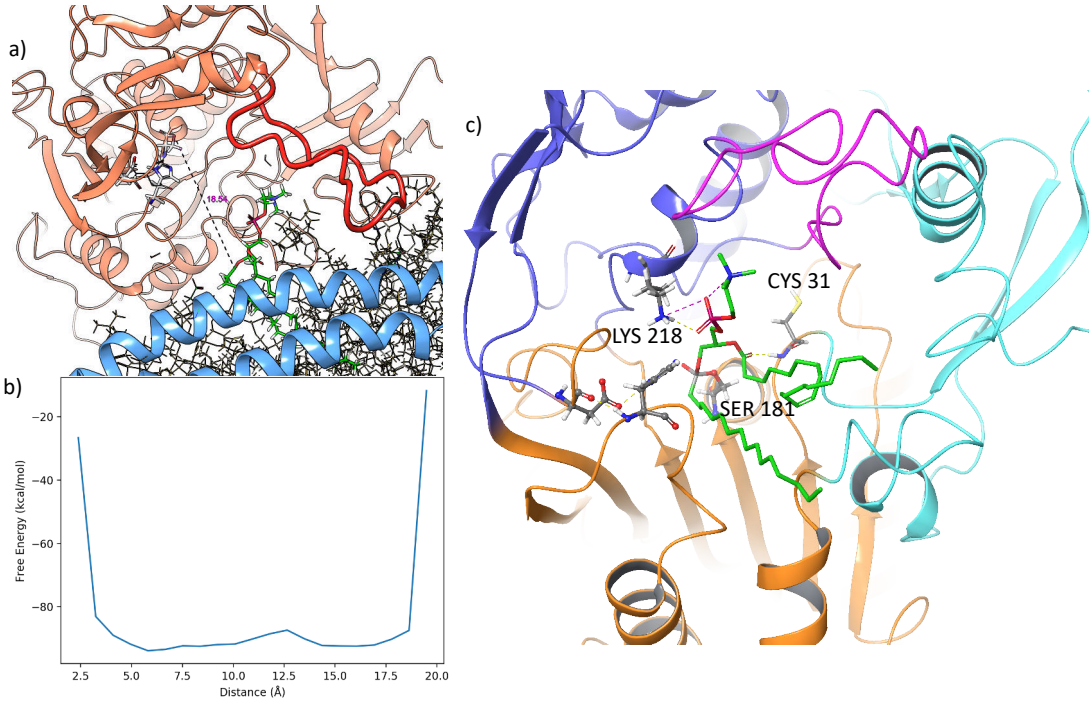

Figure 9: *LCAT acylation* — a) definition: distance between Ser181 hydroxyl group and the carboxylic carbon of the sn-2 fatty acid chain of the closest phospholipid; b) FES as function of distance CV, potential grows to infinity as the atoms are pulled too close; c) minimized structure of acylated LCAT, hydrophobicity of binding site is shown as a red surface, salt bridge between Lys218 and phosphate head group as magenta dashed line.

Downloaded from www.jlr.org at BIBLIOTECA ALBERTO MALLIANI, on December 3, 2020